Phys Chem Minerals (2003) 30: 206–216
DOI 10.1007/s00269-003-0309-3

ORIGINAL PAPER

C. A. McCammon · N. L. Ross

Crystal chemistry of ferric iron in (Mg,Fe)(Si,Al)O_3 majorite with implications for the transition zone

Received: 27 June 2002 / Accepted: 1 February 2003

Abstract Fifteen samples of (Mg,Fe)SiO_3 majorite with varying Fe/Mg composition and one sample of (Mg,Fe)(Si,Al)O_3 majorite were synthesized at high pressure and temperature under different conditions of oxygen fugacity using a multianvil press, and examined ex situ using X-ray diffraction and Mössbauer and optical absorption spectroscopy. The relative concentration of Fe^{3+} increases both with total iron content and increasing oxygen fugacity, but not with Al concentration. Optical absorption spectra indicate the presence of Fe^{2+}–Fe^{3+} charge transfer, where band intensity increases with increasing Fe^{3+} concentration. Mössbauer data were used in conjunction with electron microprobe analyses to determine the site distribution of all cations. Both Al and Fe^{3+} substitute on the octahedral site, and charge balance occurs through the removal of Si. The degree of Mg/Si ordering on the octahedral sites in (Mg,Fe)SiO_3 majorite, which affects both the c/a ratio and the unit cell volume, is influenced by the thermal history of the sample. The Fe^{3+} concentration of (Mg,Fe)(Si,Al)O_3 majorite in the mantle will reflect prevailing redox conditions, which are believed to be relatively reducing in the transition zone. Exchange of material across the transition boundary to (Mg,Fe)(Si,Al)O_3 perovskite would then require a mechanism to oxidize sufficient iron to satisfy crystal-chemical requirements of the lower-mantle perovskite phase.

Keywords Mössbauer spectroscopy · Optical absorption spectroscopy · Crystal structure, Garnet

C. A. McCammon (✉)
Bayerisches Geoinstitut, Universität Bayreuth,
95440 Bayreuth, Germany
e-mail: catherine.mccammon@uni-bayreuth.de
Tel.: +49-(0)921–553709
Fax: +49-(0)921-553769

N. L. Ross
Department of Geological Sciences, Virginia Tech,
Blacksburg, Virginia 24061, USA

Introduction

Mineral phases in the Earth's transition zone and lower mantle are dominated by components in the system MgO–SiO_2, which account for more than 80% of the chemical composition of these regions. Iron is the next most abundant element, but due to its nature as a transition element with the ability to exist in multiple valence states, its effect on physical and chemical properties can be greater than its abundance would suggest. The presence of even small amounts of Fe^{3+} can have significant effects on the physical and chemical properties, since Fe^{3+} affects the electrostatic charge balance and equilibrium defect concentration. Properties highly sensitive to such effects include sub- and supersolidus phase relations, trace-element partitioning, electrical conductivity, diffusivity, the nature of volatile species and mechanical behaviour. The effect of Fe^{3+} on these properties depends on both its concentration and its distribution over crystallographic sites in the crystal structure, and possibly on collateral effects such as vacancy concentration and distribution. An ongoing project at the Bayerisches Geoinstitut has been to characterize the nature of iron in transition-zone and lower-mantle phases, particularly with regard to the effect on physical and chemical properties. This paper focuses on (Mg,Fe)(Si,Al)O_3 majorite, which is believed to be a significant component in the transition zone and shallow lower-mantle regions (e.g., Irifune and Ringwood 1987; Ito and Takahashi 1987).

Garnet occurs in the upper mantle predominantly with composition $(Mg,Fe,Ca)_3Al_2Si_3O_{12}$, where silicon is exclusively in tetrahedral coordination. With increasing pressure, however, (Mg,Ca,Fe)SiO_3 pyroxenes become increasingly soluble in the garnet phase, introducing the component $(Mg,Fe)_3(Mg,Fe,Si)_2Si_3O_{12}$. In this majorite component, named after the mineral with (Mg,Fe)SiO_3 composition and the cubic garnet structure (Smith and Mason 1970), the octahedral sites are filled by Mg, Fe and Si. The end–member $MgSiO_3$

majorite is tetragonal, with a slight distortion from cubic symmetry that has been attributed to ordering of Mg and Si on the octahedral sites (Angel et al. 1989). The addition of Al to $MgSiO_3$ tetragonal majorite stabilizes cubic symmetry, presumably due to increased disorder of cations on the octahedral site (Hatch and Ghose 1989). Although the end member $FeSiO_3$ majorite is not stable, the solid-solution $Fe_3Al_2Si_3O_{12}$–$Fe_4Si_4O_{12}$ has been shown to extend to at least 40 mol% $FeSiO_3$ (Akaogi and Akimoto 1977). There have been several studies in the system $MgSiO_3$–$FeSiO_3$ majorite, focusing primarily on phase stability and crystal structure (Kato 1986; Matsubara et al. 1990; Ohtani et al. 1991; Tomioka et al. 2002). O'Neill et al. (1993a) have shown that even at its minimum f_{O_2} stability limit, $(Mg,Fe)SiO_3$ majorite contains measurable Fe^{3+}, which raises the question as to how it affects its physical and chemical behaviour.

Recent studies have shown that addition of Al to $(Mg,Fe)SiO_3$ perovskite stabilizes Fe^{3+} due to the favourable energetics of coupled substitution (McCammon 1997; Lauterbach et al. 2000). The garnet structure has many similarities with the perovskite structure, raising the possibility that similar behaviour might occur in majorite. This would have important implications for the transition zone, where the majority of Al is concentrated in majorite.

In this study we have synthesized a series of $(Mg,Fe)SiO_3$ and $(Mg,Fe)(Si,Al)O_3$ majorite samples under varying conditions of oxygen fugacity, and studied them using Mössbauer spectroscopy, optical absorption spectroscopy, X-ray diffraction and the electron microprobe. The results provide insight into the crystal chemistry of majorite in the transition zone.

Experimental

Orthopyroxene starting materials for $(Mg,Fe)(Si,Al)O_3$ majorite were synthesized from powder mixtures of MgO, SiO_2, Al_2O_3, Fe_2O_3 and Fe, where the latter two were partly enriched in ^{57}Fe. Experiments were run in the piston-cylinder apparatus using Ag capsules at 2 GPa and 1000 °C for approximately 20 h. Mössbauer spectroscopy showed that the orthopyroxene-rich starting materials contained no Fe^{3+}. Excess SiO_2 (approximately 2% by weight) was mixed with all starting materials to inhibit the formation of $(Mg,Fe)_2SiO_4$ phases during the multianvil experiments.

The $(Mg,Fe)(Si,Al)O_3$ majorite samples were synthesized using a multianvil press with a $LaCrO_3$ heater assembly and $W_{75}Re_{25}/W_{97}Re_{97}$ thermocouple at Bayerisches Geoinstitut. Run conditions are listed in Table 1. Different oxygen fugacity environments were imposed on the sample through the use of different capsule materials (Rubie 1999): (1) Fe metal capsule with a thin layer of unenriched Fe powder added at the bottom of the capsule; (2) Mo capsule; (3) Re capsule; (4) Re capsule with a thin layer of ReO_2 powder added at the bottom of the capsule. Part of the pellets from the run products were crushed in an agate mortar and the resulting powder was mounted on a cellophane foil that was used for both Mössbauer and X-ray experiments. The remaining chips were made into polished thin sections for the electron microprobe, and doubly polished plates for optical absorption spectroscopy. Further details of the samples are given in Table 1.

Table 1 Details of $(Mg,Fe)(Si,Al)O_3$ majorite synthesis, chemical composition and cell parameters

Sample no	P (GPa)	T (°C)	Time (min)	x_{Fe}[a,b]	x_{Mg}[a,b]	x_{Si}[a,b]	x_{Al}[a,b]	Capsule	Added to run	Products[c]	a (Å)	c (Å)	V (Å^3)
U203	18	1800	30	*0.10(2)*	*0.90(2)*	*1.00(1)*	–	Re		gt	11.5328(3)	11.4444(3)	1522.2(1)
U307	18	1800	15	*0.20(2)*	*0.80(2)*	*1.00(1)*	–	Mo		gt	11.5291(10)	11.4458(10)	1521.4(3)
U319	18	1800	15	*0.10(2)*	*0.90(2)*	*1.00(1)*	–	Mo		gt	11.5307(5)	11.4412(5)	1521.2(1)
U526	18	1900[d]	5	*0.15(2)*	*0.85(2)*	*1.00(1)*	–	Fe	Fe	gt(sp,Fe)	11.5282(9)	11.4659(12)	1523.8(3)
U1038	19	1900[d]	20	0.152(6)	0.855(13)	0.997(7)	–	Re	ReO_2	gt	11.5300(10)	11.4520(10)	1522.4(3)
U1089	20	1820[d]	23	*0.15(2)*	*0.85(2)*	*1.00(1)*	–	Fe	Fe	gt(sp)	n.d.	n.d.	n.d.
U1127	19	1900[d]	30	0.059(6)	0.936(24)	1.003(8)	–	Fe	Fe	gt	11.5236(5)	11.4327(8)	1518.2(2)
U1146	19	1900	38	0.055(4)	0.951(9)	0.997(7)	–	Re		gt(sp)	11.5254(5)	11.4350(8)	1519.0(2)
U1161	19	1900	30	0.049(3)	0.962(5)	0.994(6)	–	Re	ReO_2	gt	11.5245(4)	11.4377(6)	1519.1(1)
U1120	19	1900[d]	28	0.115(12)	0.862(19)	1.011(18)	–	Fe	Fe	gt(sp,Fe)	11.5254(8)	11.4439(12)	1520.1(3)
U1116	19	1900[d]	42	0.114(4)	0.882(12)	1.002(5)	–	Re		gt	11.5279(7)	11.4472(11)	1521.2(2)
U1147	19	1900[d]	16	0.100(3)	0.890(9)	1.005(6)	–	Re	ReO_2	gt(sp)	11.5294(9)	11.4499(12)	1522.0(3)
U1217	19	1900	17	0.166(4)	0.835(5)	1.000(5)	–	Fe	Fe	gt(sp,Fe)	11.5250(16)	11.4557(17)	1521.6(5)
U1219	19	1900[d]	25	0.178(3)	0.819(13)	1.002(11)	–	Re		gt	11.5321(4)	11.4465(6)	1522.3(1)
U1220	19	1900	25	0.166(4)	0.839(6)	0.998(5)	–	Re	ReO_2	gt(sp)	11.5357(5)	11.4500(7)	1523.7(2)
U2144	19	1900	30	*0.14(1)*	*0.84(1)*	*0.93(1)*	*0.09(1)*	Re	ReO_2	gt(wd)	11.4915(4)	–	1517.5(2)

[a] Numbers *in italics* are nominal compositions based on the starting material
[b] Based on three oxygen anions
[c] Minor phases in parentheses (*sp* ringwoodite; *Fe* metallic iron; *wd* wadsleyite). All samples contained stishovite
[d] Estimated from power based on previous experiments under similar conditions

The (Mg, Fe)(Si, Al)O_3 majorite synthesis experiments were carried out in two series of high-pressure experiments. Runs U203 through U1038 were carried out in the period 1990–1994 while the multianvil press was located in the "farmhouse" barracks at the Bayerisches Geoinstitut, while runs U1089–U1220 and run U2144 were carried out on the same press after moving the equipment to the new building. Some preliminary results from runs U203 through U526 have already been presented (O'Neill et al. 1993a, b), and the sample from run U1038 was studied using optical absorption spectroscopy by Keppler and McCammon (1996).

X-ray powder diffraction data were obtained using monochromated Co Kα_1 radiation in transmission mode. Data were collected from 30° to 125° over 2θ angles, and showed the dominant presence of majorite, with minor amounts in various samples of stishovite, Fe, ReO_2, $(Mg,Fe)_2SiO_4$ ringwoodite and $(Mg,Fe)_2SiO_4$ wadsleyite. We used the lines corresponding to stishovite as an internal calibration standard ($a = 4.1790$ Å, $c = 2.6649$ Å). The X-ray diffraction data of all (Mg,Fe) SiO_3 majorite samples were fit to a tetragonal unit cell, while the (Mg,Fe)(Si,Al)O_3 majorite data were fit to a cubic cell (Table 1).

Mössbauer spectra were recorded at 293 and 80 K in transmission mode on a constant-acceleration Mössbauer spectrometer using a nominal 1.85 GBq ^{57}Co source in a 6-mm Rh matrix. The velocity scale was calibrated relative to metallic iron using the positions certified for National Bureau of Standards standard reference material no. 1541; line widths of 0.28 mms^{-1} for the outer lines of α-Fe were obtained at room temperature. Mössbauer spectra were collected with the absorber at 80 K (source at 293 K) using a cold-finger cryostat capable of controlling to ± 0.5 K. The commercially available fitting program NORMOS 90 written by R.A. Brand was used to fit the spectra.

Optical and near-infrared absorption measurements were carried out on doubly polished grain aggregates of majorite up to 70 μm thickness. The spectra with low iron concentration (U1127–U1147) were too weak to measure, so spectra could only be collected from samples with $x_{Fe} > 0.15$ (U1217, U1219 and U1220). Sample U2144 could not be measured due to the presence of wadsleyite on a fine scale. All measurements were carried out with a beam diameter of 100 μm using a Bruker infrared microscope coupled with a Bruker IFS 120 HR high-resolution FTIR spectrometer. Several hundred scans with 4-cm^{-1} resolution were accumulated in the spectral ranges from 1000 to 10 000 cm^{-1} (CaF_2 beam splitter, tungsten source, MCT detector), 9000 to 15 000 cm^{-1} (quartz beam splitter, tungsten source, Si diode detector) and 12 500 to 25 000 cm^{-1} (quartz beam splitter, xenon arc source, Si diode detector) and merged to produce the final spectrum.

Results

Mössbauer spectroscopy

Mössbauer spectra of (Mg,Fe)(Si,Al)O_3 majorite are similar to those already reported in the literature (O'Neill et al. 1993a, b), and consist of a dominant quadrupole doublet superimposed with several less intense peaks (Fig. 1). The use of enriched ^{57}Fe enabled high signal-to-noise ratios to be obtained despite the small amounts of sample available, but also introduced thickness effects. We therefore fitted spectra using the full transmission integral to account for these effects. The dimensionless effective thickness of each sample was calculated from sample geometry and chemical composition. We fitted three doublets to each spectrum, two corresponding to Fe^{2+} and one to Fe^{3+}. In certain spectra we also fitted a doublet corresponding to $(Mg,Fe)_2SiO_4$ ringwoodite or wadsleyite, and a sextet corresponding to Fe metal. The component areas and

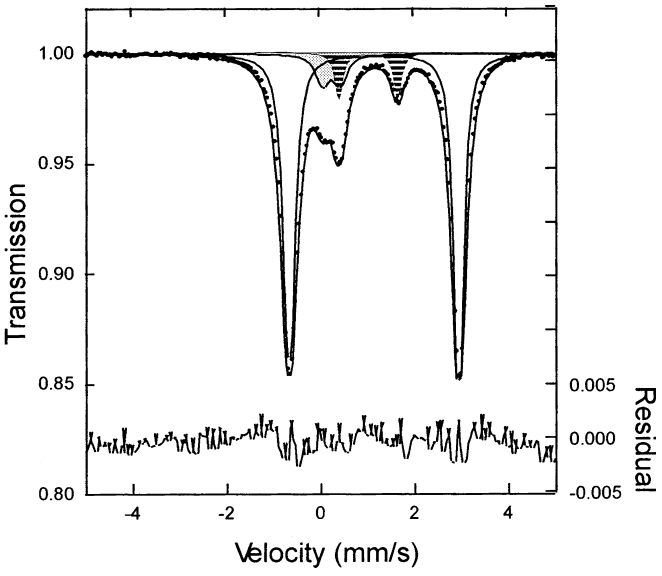

Fig 1 Room-temperature Mössbauer spectrum of $^{57}Fe_{0.1}Mg_{0.9}SiO_3$ majorite (Run U203). The spectrum was fitted using the full transmission integral, and shows doublets corresponding to dodecahedral Fe^{2+} (*unshaded*), octahedral Fe^{2+} (*striped*) and Fe^{3+} (*grey*)

widths of the doublet corresponding to dodecahedral Fe^{2+} were allowed to vary, since there is minimal overlap of the dodecahedral Fe^{2+} doublet with other components in the spectrum, and large residuals were obtained when they were constrained to be equal. The unequal widths and areas most likely reflect a small degree of next-nearest-neighbour effects (e.g., Angel et al. 1998) and anisotropic recoil-free fraction (Geiger et al. 1992). All other doublets were constrained to have equal component areas and widths, and the sextet was constrained to have equal component widths and areas in the ratio 3:2:1:1:2:3. In a few spectra, some hyperfine parameters had to be constrained due to weak peak intensity. Hyperfine parameters are listed in Table 2.

Relative areas were corrected for effects due to different site recoil-free fractions using the Debye model (e.g., McCammon 1998). We used Mössbauer Debye temperatures of 340 K for Fe^{2+} and 400 K for Fe^{3+} (Amthauer et al. 1976; DeGrave and van Alboom 1991). The agreement between the corrected relative areas calculated for spectra recorded at 293 K compared to those at 80 K (where differing recoil-free fraction effects are smaller) is within experimental error (Table 2).

The hyperfine parameters for (Mg,Fe)(Si,Al)O_3 majorite fall into three distinct ranges, and there is no significant variation between samples with and without Al (Fig. 2). Based on data in the literature (e.g., Amthauer et al. 1976), the two Fe^{2+} doublets can be unambiguously assigned to the dodecahedral and octahedral sites in the structure. The values of centre shift and quadrupole splitting for the Fe^{2+} doublets do not vary significantly over the sample set that we studied. In contrast, the centre shift of the Fe^{3+} doublet shows a systematic increase as $Fe^{3+}/\sum Fe$ becomes larger (Fig. 3). The most likely site assignment for Fe^{3+} is the octahedral site.

Table 2 Hyperfine parameters of $(Mg,Fe)(Si,Al)O_3$ majorite determined from Mössbauer spectra. *CS* centre shift; *QS* quadrupole splitting; Γ full width at half maximum; *A* relative area

Run no.	$^{[8]}Fe^{2+}$			$^{[6]}Fe^{2+}$			Fe^{3+}			$^{[8]}Fe^{2+}$	$^{[6]}Fe^{2+}$	Fe^{3+}	$Fe^{3+}/\sum Fe^{e}$	$^{[6]}Fe^{2+}/\sum Fe^{2+}{}_{e}$
	CS[a] (mm s^{-1})	QS (mm s^{-1})	Γ[b] (mm s^{-1})	CS[a] (mm s^{-1})	QS (mm s^{-1})	Γ (mm s^{-1})	CS[a] (mm s^{-1})	QS[c] (mm s^{-1})	Γ[c] (mm s^{-1})	A[d]	A[d]	A[d]		
293 K spectra:														
U203	1.266(5)	3.611(5)	0.27	1.144(17)	1.254(34)	0.19	0.36(3)	0.36(3)	0.33	0.80(2)	0.07(1)	0.13(1)	0.12(1)	0.08(1)
U307	1.263(5)	3.583(5)	0.35	1.151(15)	1.258(28)	0.28	0.22(1)	*0.36*	0.50	0.82(1)	0.09(2)	0.09(1)	0.08(1)	0.10(2)
U319	1.259(5)	3.600(5)	0.29	1.132(5)	1.265(6)	0.22	0.22(1)	0.42(3)	*0.40*	0.82(1)	0.11(2)	0.08(1)	0.07(1)	0.11(1)
U526	1.271(5)	3.609(5)	0.20	1.160(52)	1.279(99)	0.23	0.22(11)	0.35(9)	0.32	0.67(4)	0.07(1)	0.08(1)	0.09(1)	0.10(1)
U1038	1.265(5)	3.587(5)	0.24	1.153(16)	1.275(9)	0.20	0.36(1)	0.37(1)	0.33	0.73(4)	0.04(2)	0.23(2)	0.22(2)	0.05(2)
U1089	1.238(5)	3.535(5)	0.19	1.110(24)	1.300(63)	0.30	0.32(4)	0.39(7)	0.36	0.71(2)	0.09(1)	0.10(1)	0.10(1)	0.11(1)
U1127	1.249(5)	3.583(5)	0.16	1.131(5)	1.272(9)	0.23	0.19(10)	0.33(11)	*0.40*	0.81(7)	0.06(2)	0.03(1)	0.03(2)	0.06(2)
U1146	1.258(5)	3.602(5)	0.21	1.114(5)	1.306(60)	0.27	0.32(1)	0.46(9)	*0.40*	0.83(2)	0.07(2)	0.10(1)	0.09(1)	0.07(2)
U1161	1.258(5)	3.601(5)	0.22	1.147(54)	1.281(75)	0.35	0.31(3)	0.40(1)	*0.40*	0.81(1)	0.06(1)	0.13(1)	0.12(1)	0.07(1)
U1120	1.259(5)	3.596(5)	0.20	1.139(5)	1.255(5)	0.20	0.28(2)	0.30(3)	0.43	0.83(3)	0.07(2)	0.05(1)	0.05(1)	0.08(2)
U1116	1.251(5)	3.569(5)	0.19	1.134(5)	1.262(5)	0.23	0.30(2)	0.33(2)	0.37	0.88(5)	0.06(2)	0.06(3)	0.06(3)	0.06(2)
U1147	1.259(5)	3.587(5)	0.22	1.161(14)	1.254(63)	0.26	0.33(1)	0.36(1)	0.40	0.79(5)	0.04(2)	0.16(2)	0.15(2)	0.05(3)
U1217	1.262(5)	3.588(5)	0.20	1.160(5)	1.245(7)	0.26	0.30(1)	0.32(1)	0.28	0.82(4)	0.08(2)	0.06(1)	0.06(1)	0.09(2)
U1219	1.260(5)	3.595(5)	0.21	1.148(5)	1.253(12)	0.21	0.32(1)	0.35(2)	0.35	0.85(6)	0.06(2)	0.09(2)	0.08(2)	0.06(2)
U1220	1.261(5)	3.593(5)	0.22	1.144(22)	1.270(44)	0.20	0.36(2)	0.36(2)	0.31	0.80(6)	0.05(2)	0.13(3)	0.12(3)	0.06(2)
U2144	1.271(5)	3.559(5)	0.18	–	–	–	0.31(1)	0.39(1)	0.34	0.67(5)	0.00(1)	0.12(1)	0.14(1)	0.00(1)
80 K spectra:														
U203	1.403(5)	3.744(5)	0.32	1.264(5)	1.714(9)	0.30	0.44(1)	0.40(1)	0.34	0.79(2)	0.09(1)	0.13(1)	0.13(1)	0.10(1)
U307	1.405(5)	3.730(5)	0.29	1.247(5)	1.798(8)	0.37	0.33(1)	0.40(1)	0.44	0.79(3)	0.11(2)	0.10(1)	0.10(1)	0.12(2)
U319	1.405(5)	3.730(5)	0.34	1.253(5)	1.726(5)	0.33	0.38(1)	0.39(1)	0.36	0.80(2)	0.12(1)	0.08(1)	0.08(1)	0.13(1)

[a] Relative to metallic iron
[b] Average value (component widths were not constrained to be equal)
[c] *Values in italics* were held fixed during fitting
[d] Areas adding to less than 1.0 contained additional phases (ringwoodite, wadsleyite, metallic iron)
[e] corrected for recoil-free fraction effects

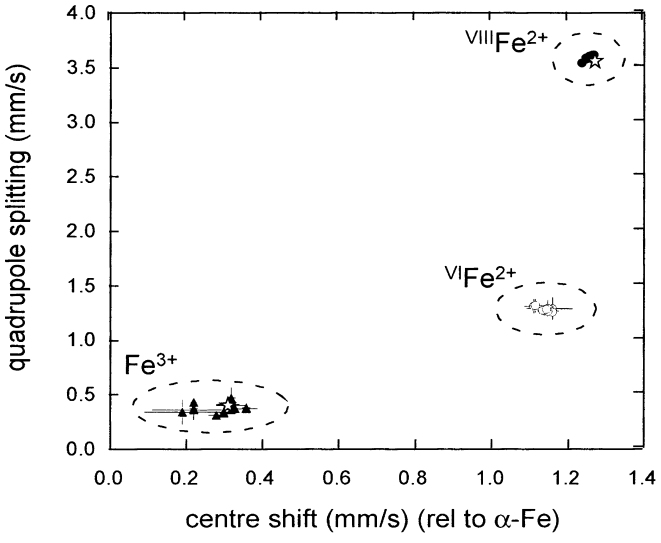

Fig. 2 Variation of quadrupole splitting with centre shift (relative to α-Fe) for all doublets fitted to $(Mg,Fe)(Si,Al)O_3$ majorite spectra. Data for $(Mg,Fe)SiO_3$ majorite is indicated by *solid circles* ($^{[8]}Fe^{2+}$), *open circles* ($^{[6]}Fe^{2+}$) and *triangles* (Fe^{3+}), while corresponding data for the $(Mg,Fe)(Si,Al)O_3$ majorite sample are indicated by *stars*

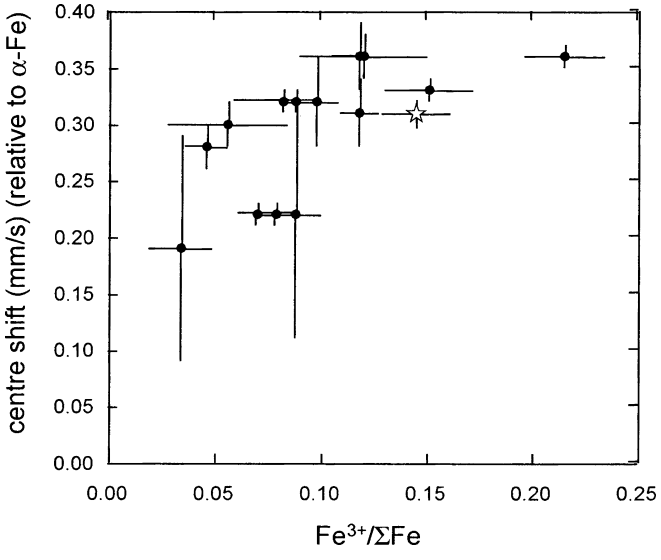

Fig. 3 Variation of centre shift (relative to α-Fe) with $Fe^{3+}/\sum Fe$ for the Fe^{3+} doublet in $(Mg,Fe)SiO_3$ majorite (*solid circles*) and $(Mg,Fe)(Si,Al)O_3$ majorite (*star*) spectra. The increase most likely reflects increasing Fe–O distance in the octahedral site

Values of the centre shift are consistent with cation–oxygen distances up to approximately 2.0 Å (McCammon 1996), and the increase in centre shift is consistent with an inferred increase in mean Fe–O distance with increasing substitution of Fe^{3+}, based on the larger ionic radius of Fe^{3+} compared to Si. The other site possibility for Fe^{3+} is the tetrahedral site, but this would appear unlikely based on the high centre shifts and the fact that tetrahedral Fe^{3+} occurs in garnet only in rare circumstances where a cation such as Sn, Zr or Ti has preferentially filled the octahedral sites (Amthauer et al. 1976).

The relative concentration of Fe^{3+} in $(Mg,Fe)(Si,Al)O_3$ majorite increases both with total iron content and oxygen fugacity (Fig. 4). Similar behaviour has been observed for other iron-containing minerals, for example (Mg,Fe)O (Speidel 1967), and reflects the driving force of the reaction $2FeO + 1/2\ O_2 \rightarrow Fe_2O_3$ over crystal-chemical considerations in determining the relative Fe^{3+} concentration in majorite. The value of $Fe^{3+}/\sum Fe$ for the $(Mg,Fe)(Si,Al)O_3$ majorite sample is not significantly different from results obtained from Al-free samples under the same redox conditions (Re capsule with ReO_2 added), indicating that there is no enhancement of Fe^{3+} concentration in majorite with Al concentration comparable to behaviour in $(Mg,Fe)(Si,Al)O_3$ perovskite.

Two approximately linear trends for $(Mg,Fe)SiO_3$ majorite are defined, one for samples synthesized in Fe capsules with excess Fe added, and one for samples synthesized in Re capsules with excess ReO_2 added (Fig. 4). During these runs oxygen fugacity was constrained by the "buffering" phase within limits that were usually maintained for the duration of the run. Redox equilibrium was most likely reached in these runs based on the consistency of $Fe^{3+}/\sum Fe$ values. Samples run with no "buffering" phase present, however, were subject to conditions of oxygen fugacity that probably varied during the experiment, since the sample capsule material alone was most likely not able to influence local redox conditions sufficiently. Results from these runs, therefore, cannot be used to infer a relation between Fe^{3+} and oxygen fugacity.

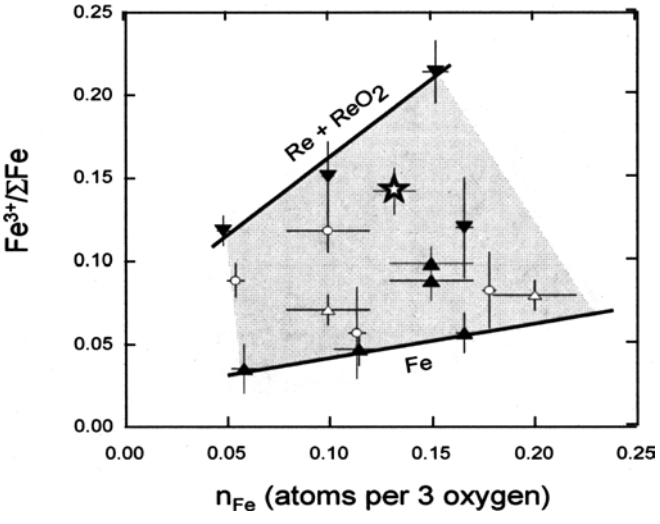

Fig. 4 Effect of oxygen fugacity on $Fe^{3+}/\sum Fe$ for $(Mg,Fe)(Si,Al)O_3$ majorite. The *grey area* indicates the range of experimental data, where the minima and maxima (*solid lines*) are defined by equilibrium with metallic Fe and with Re/ReO_2, respectively. Symbols are as follows for $(Mg,Fe)SiO_3$ majorite: *solid triangles* Fe capsules + powder Fe; *open circles* Mo capsules; *open triangles* Re capsules; *solid inverted triangles* Re capsules with powder ReO_2; for $(Mg,Fe)(Si,Al)O_3$ majorite: *star* Re capsule with powder ReO_2

Optical absorption spectroscopy

The optical and near infrared spectra of $(Mg_{0.85}Fe_{0.15})SiO_3$ majorites synthesized with Fe, Re and $Re + ReO_2$ display the same features as the spectrum obtained by Keppler and McCammon (1996) for $(Mg_{0.86}Fe_{0.14})SiO_3$ majorite that was synthesized at 19 GPa and 1900 °C in a Re capsule with a trace of ReO_2. A merged, unpolarized optical and near-infrared absorption spectrum is shown in Fig. 5 before and after subtraction of an almost linear background. Similarly to the study of Keppler and McCammon (1996), we deconvoluted each spectrum into seven Gaussian components, which was the minimum required to achieve a satisfactory fit of the spectrum (Fig. 6). Spectra were merged and fit several times to test the reproducibility of the peak-fitting algorithms. In all cases, seven Gaussian components were required to reproduce the spectrum, and individual peak positions varied within 100–200 cm^{-1} of the peak positions shown in Table 3.

The positions of the peaks show generally reasonable agreement with those determined by Keppler and McCammon (1996); hence the same band assignments have been used in this study. Three bands located at approximately 5550, 6200 and 8400 cm^{-1} are assigned to the transitions of Fe^{2+} in the distorted dodecahedral site (Table 3), although we note that these bands occur at wavenumbers higher than those reported by Keppler and McCammon (1996). A weak band near 9400 cm^{-1} is assigned to Fe^{2+} in the octahedral site and is similar to the value reported by Keppler and McCammon (1996). The dominant feature of all spectra is a very broad and intense

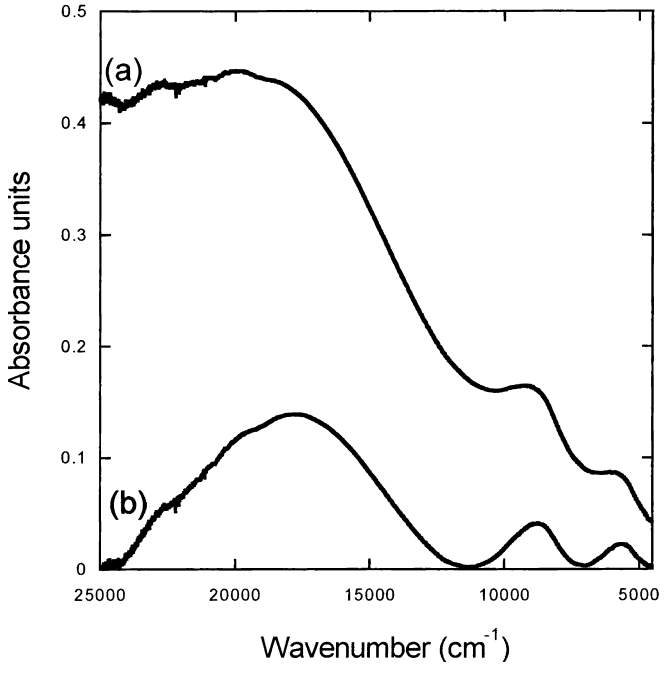

Fig. 5 Unpolarized optical and near-infrared absorption spectrum of $(Mg_{0.85}Fe_{0.15})SiO_3$ majorite from run U1220 (a) before and (b) after subtraction of an almost linear baseline

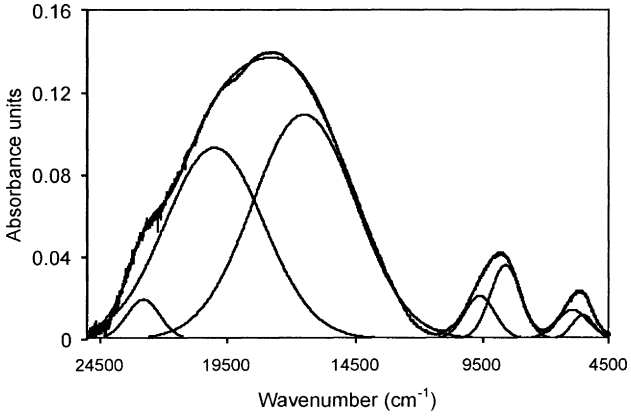

Fig. 6 Unpolarized optical and near-infrared absorption spectrum of $(Mg_{0.85}Fe_{0.15})SiO_3$ majorite from run U1220 illustrating the deconvolution into seven Gaussian components

absorption system between 12 000 and 22 000 cm^{-1}. The overall shape of this feature suggests that at least two Gaussian components must be present. Deconvolution of this broad absorption feature yielded two components centred near 16 300 and 20 000 cm^{-1} with widths of 5000 cm^{-1}, consistent with $Fe^{2+} \rightarrow Fe^{3+}$ intervalence charge transfer bands (Mattson and Rossman 1987; Burns 1993). Lastly, a weak band is observed near 23 000 cm^{-1} which is assigned to the Fe^{3+} transition, ${}^6A_{1g} \rightarrow {}^4A_{1g}, {}^4E_g$.

Figure 7 illustrates a crystal-field diagram for dodecahedral Fe^{2+} in $(Mg_{0.85}Fe_{0.15})SiO_3$ majorite indicating the interpretation of the observed absorption bands. The crystal-field splitting, Δ, of Fe^{2+} in the dodecahedral site of majorite can be calculated from the three absorption bands, v_1, v_2 and v_3, by the relationship: $\Delta = 1/3\ (v_1 + v_2 + v_3)\ -1/2\ \delta$, where δ is the splitting of the ground state (White and Moore 1972). Since δ cannot be obtained from optical absorption spectra, we used the approximation of Keppler and McCammon (1996) of $\delta = 1000$ cm^{-1}.

The crystal field stabilization energy (CFSE) is given by $(3/5\Delta + 1/2\delta)$. The CFSEs calculated on the basis of the data given in Table 3 are 4286 cm^{-1} (U1217), 4249 cm^{-1} (U1219) and 4211 cm^{-1} (U1220), which are all greater than the value of 3930 cm^{-1} reported by Keppler and McCammon (1996). The difference is due to the position of v_1, which is approximately 1000 cm^{-1} higher than that reported by Keppler and McCammon (1996). The difference in frequencies, v_3–v_1, of the ${}^5T_{2g}$ levels provides a measure of the dodecahedral site distortion, and is approximately 3000 cm^{-1} for all of the $(Mg_{0.85}Fe_{0.15})SiO_3$ majorites in the present study. This value is significantly lower than the frequency difference of 3539 cm^{-1} reported by Keppler and McCammon (1996), which suggests that the site distortion and occupancies of the dodecahedral sites differ between the majorites synthesized in the two studies. One possibility to account for the differences is effects due to different run conditions, particularly the quench rate.

The CFSE of octahedral Fe^{2+} is estimated from the single peak observed around 9400 cm^{-1} (Table 3).

Table 3 Optical and near-infrared bands of $(Mg_{0.85}Fe_{0.15})SiO_3$ majorite assuming Gaussian lineshapes

Run 1217		Run U1219		Run U1220		Peak assignment
Position (cm^{-1})	Width[a] (cm^{-1})	Position (cm^{-1})	Width[a] (cm^{-1})	Position (cm^{-1})	Width[a] (cm^{-1})	
5560	1224	5534	990	5532	980	$^{[8]}Fe^{2+}$ ($^5E_g \rightarrow {}^5T_{2g}$)
6463	962	6238	970	5947	1481	$^{[8]}Fe^{2+}$ ($^5E_g \rightarrow {}^5T_{2g}$)
8405	1028	8475	1300	8577	1398	$^{[8]}Fe^{2+}$ ($^5E_g \rightarrow {}^5T_{2g}$)
9311	1810	9372	1234	9585	1394	$^{[6]}Fe^{2+}$ ($^5T_{2g} \rightarrow {}^5E_g$)
16293	5019	16210	4999	16471	4731	$^{[8]}Fe^{2+} \rightarrow {}^{[6]}Fe^{3+}$ CT[b]
19932	5057	19964	4842	19986	4562	$^{[8]}Fe^{2+} \rightarrow {}^{[6]}Fe^{3+}$ CT[b]
22931	1658	22786	1856	22780	1526	$^{[6]}Fe^{3+}$ ($^6A_{1g} \rightarrow {}^4A_{1g}$, ^4E_g)

[a] Full width at half height
[b] Charge transfer

Normally, two bands due to Jahn–Teller distortion would be expected (e.g., Burns 1993), but due to the regularity of the octahedral sites in the tetragonal garnet structure (Angel et al. 1989), the Jahn–Teller splitting must be small and the crystal-field splitting will be close to the observed band frequency (Keppler and McCammon 1996). The CFSEs of octahedral Fe^{2+} in majorite determined in this study are 3724 cm^{-1}, 3749 cm^{-1} and 3834 cm^{-1} for runs U1217, U1219 and U1220, respectively, and are in good agreement with the value of 3736 cm^{-1} determined by Keppler and McCammon (1996).

Discussion

Site distribution, structure and charge balance

The site distribution of all cations can be determined based on the Mössbauer data and the chemical composition. The corrected relative areas give the relative distribution of Fe^{2+} between the dodecahedral and octahedral site, and of Fe^{3+} on the octahedral site, and combined with the total iron from the microprobe data (Table 1), were used to determine the number of iron atoms on each site. Next, the remaining dodecahedral sites were filled with magnesium atoms, and the remainder of magnesium was assigned to octahedral sites. The amount of silicon on octahedral sites was calculated based on charge balance and assuming full occupation of tetrahedral sites with silicon. The resulting site distributions (based on 12 oxygen anions) show all $(Mg,Fe)(Si,Al)O_3$ majorite samples to be stoichiometric within experimental uncertainty (Table 4).

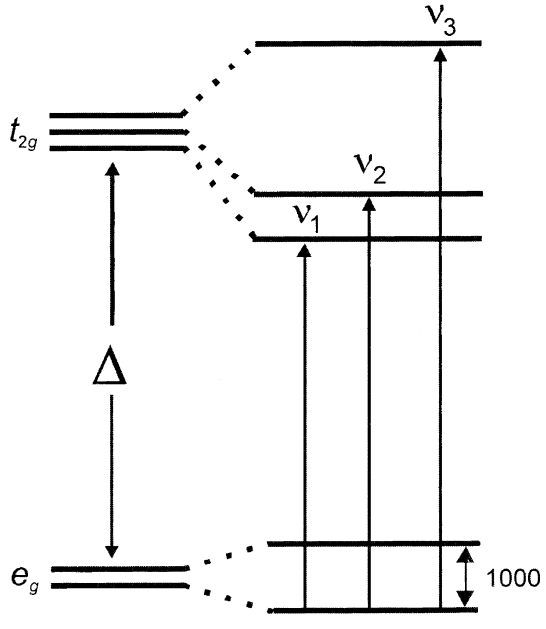

Fig. 7 Energy-level diagram for Fe^{2+} in a dodecahedral site in majorite

The addition of Al to $(Mg,Fe)SiO_3$ majorite does not stabilize Fe^{3+} in the garnet structure, in contrast to the behaviour of $(Mg,Fe)(Si,Al)O_3$ perovskite. This can be understood on the basis of cation substitution. The strong preference of $(Mg,Fe)(Si,Al)O_3$ perovskite for Fe^{3+} in the presence of Al is based on the energetically favourable coupled substitutions (1) $^{[8-12]}Mg^{2+} + {}^{[6]}Si^{4+} \leftrightarrow {}^{[8-12]}Fe^{3+} + {}^{[6]}Al^{3+}$; and (2) $^{[6]}Si^{4+} \leftrightarrow {}^{[6]}Fe^{3+} + {}^{[6]}Al^{3+} + V_O^{2+}$ (Richmond and Brodholt 1998). The first requires Fe^{3+} and Al^{3+} to occupy different sites, and the second requires the creation of an oxygen vacancy. In the garnet structure, neither of these possibilities is energetically favoured, since Al and Fe^{3+} occupy only octahedral sites, and significant numbers of oxygen vacancies have not been observed (Table 4). In $(Mg,Fe)(Si,Al)O_3$ majorite, both Al and Fe^{3+} compete for the same site, which most likely inhibits the oxidation of Fe^{2+} to Fe^{3+}. Indeed, Fig. 4 demonstrates that $(Mg,Fe)(Si,Al)O_3$ majorite contains less Fe^{3+} than $(Mg,Fe)SiO_3$ majorite at the same iron concentration and under redox conditions. Thus, the concentration of Fe^{3+} in $(Mg,Fe)(Si,Al)O_3$ majorite is strongly dependent on the oxygen fugacity and not the crystal chemistry of the garnet structure, while the concentration of Fe^{3+} in $(Mg,Fe)(Si,Al)O_3$ perovskite is independent of oxygen fugacity, and is related to the favourable energetics of Fe^{3+} substitution in the presence of Al in the perovskite structure (Lauterbach et al. 2000).

The tetragonal $MgSiO_3$ majorite structure has two distinct dodecahedral sites (D1 and D2) as well as octahedral sites (Oc1 and Oc2), where Mg and Si are strongly ordered on the octahedral sites (Angel et al.

Table 4 Cation site distribution based on 12 oxygen atoms and fully occupied dodecahedral and tetrahedral cation sites in $(Mg,Fe)(Si,Al)O_3$ majorite

Run no.	$^{[8]}Mg$	$^{[8]}Fe$	$^{[6]}Mg$	$^{[6]}Fe^{2+}$	Fe^{3+}	$^{[6]}Si$	$^{[6]}Al$	$^{[6]}\sum$
U203	2.677(81)	0.323(81)	0.923(114)	0.030(8)	0.047(11)	0.988(57)	–	1.988(128)
U307	2.337(82)	0.663(82)	0.863(115)	0.074(15)	0.063(10)	0.984(57)	–	1.984(129)
U319	2.670(81)	0.330(81)	0.930(114)	0.042(11)	0.028(7)	0.993(57)	–	1.993(128)
U526	2.508(81)	0.492(81)	0.892(114)	0.055(11)	0.053(10)	0.987(57)	–	1.987(129)
U1038	2.546(28)	0.454(28)	0.873(59)	0.022(9)	0.131(13)	0.955(31)	–	1.980(68)
U1089	2.517(81)	0.483(81)	0.883(114)	0.058(11)	0.059(10)	0.985(57)	–	1.985(128)
U1127	2.788(26)	0.212(26)	0.955(100)	0.015(5)	0.008(4)	1.009(50)	–	1.987(111)
U1146	2.814(18)	0.186(18)	0.991(42)	0.015(5)	0.019(3)	0.983(21)	–	2.008(47)
U1161	2.840(13)	0.160(13)	1.010(25)	0.011(2)	0.023(2)	0.972(13)	–	2.016(28)
U1120	2.595(49)	0.405(49)	0.854(92)	0.034(11)	0.021(5)	1.040(46)	–	1.949(103)
U1116	2.595(24)	0.405(24)	0.933(53)	0.027(10)	0.025(13)	1.001(28)	–	1.986(62)
U1147	2.679(17)	0.321(17)	0.883(40)	0.017(9)	0.060(9)	1.005(20)	–	1.965(46)
U1217	2.429(21)	0.571(21)	0.912(29)	0.055(11)	0.037(8)	0.989(15)	–	1.992(35)
U1219	2.389(24)	0.611(24)	0.887(58)	0.042(14)	0.059(16)	0.992(31)	–	1.979(69)
U1220	2.448(29)	0.552(29)	0.907(38)	0.032(12)	0.080(20)	0.970(24)	–	1.990(50)
U2144	2.547(43)	0.453(43)	0.761(59)	0.000(13)	0.075(9)	0.757(30)	0.408(40)	2.001(79)

1989). Mössbauer data for Fe^{2+} on the dodecahedral site show little variation across the entire sample set, and linewidths are close to the theoretical minimum (Table 2), which would argue for preferential ordering of Fe^{2+} onto one of the dodecahedral sites. Optical absorption data from the present study suggest that the ordering may take place on the least distorted dodecahedral site, D2, in contrast to the previous study of Keppler and McCammon (1996). Mössbauer data for Fe^{2+} on the octahedral site also show little variation across the sample set, although linewidths are slightly larger, but nevertheless the data are still consistent with occupation of primarily one octahedral site. From bond length considerations, this would appear to be the Oc1 site, also favoured by magnesium (Angel et al. 1989). In contrast, hyperfine parameters for Fe^{3+} vary with Fe^{3+} concentration and linewidths are relatively large, suggesting that Fe^{3+} may occupy both the Oc1 and Oc2 sites. The large variation in centre shift with increasing Fe^{3+} concentration may indicate a shift in the relative proportions of Fe^{3+} on each type of octahedral site.

The c/a ratio of $MgSiO_3$ tetragonal majorite is related to the degree of Mg/Si ordering on the octahedral sites (Angel et al. 1989). The highest correlation in our dataset is shown by the variation of c/a with the number of iron atoms (both Fe^{2+} and Fe^{3+}) on octahedral sites, where two nearly linear trends are formed, indicating that the effect of increasing iron concentration is to reduce the deviation of the unit cell from cubic symmetry (Fig. 8). The primary difference between the data forming each trend appears to be that those with smaller slope are comprised primarily of runs from the first series (U203 to U1038), while those with larger slope mostly comprise runs from the second series (U1127 to U1220). The c/a ratio varies even for end-member $MgSiO_3$ majorite for runs from different laboratories (the value of 0.998 from Angel et al. 1989 is off-scale in Fig. 8), and has been attributed to different run conditions causing a variation in Mg/Si ordering (Angel et al. 1989). This is supported by a recent study showing differences in microtexture

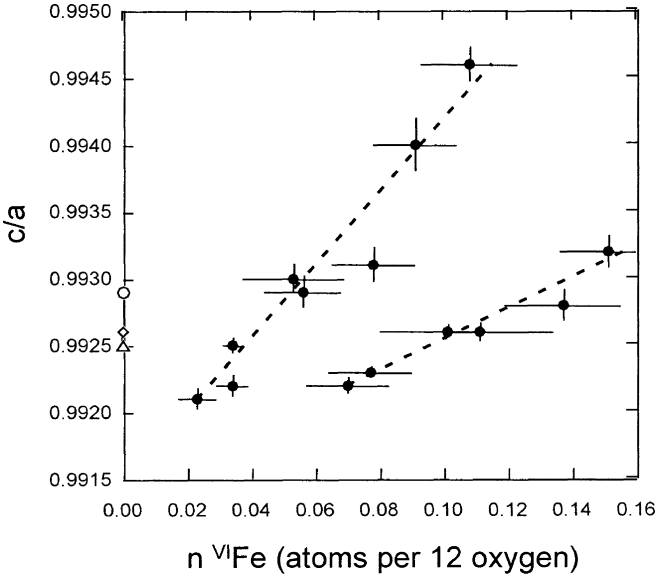

Fig. 8 Variation of c/a with the total number of iron atoms on octahedral sites in $(Mg,Fe)SiO_3$ majorite. Symbols indicate data from the present work (*solid circles*), Kato and Kumazawa (1985) (*open diamond*), Matsubara et al. (1990) (*open triangle*), and Ohtani et al. (1991) (*open circle*) (*the latter three are on the y-axis*). The value from Angel et al. (1989) of 0.998 is off-scale. *Dotted lines* indicate the two approximately linear trends defined by the two different sets of high-pressure experiments

between samples quenched below and above 1950 °C, which is attributed to a cubic-tetragonal phase transition during quenching (Tomioka et al. 2002). Synthesis temperatures in the present study are close to 1950 °C; hence, relocation of the multianvil press between the two series of runs could have caused small variations that affected cation ordering. It is clear from these results that c/a ratios must be used with caution in comparing $(Mg,Fe)SiO_3$ majorite samples with different thermal histories.

The volume of the unit cell of $(Mg,Fe)SiO_3$ majorite has been reported to increase with increasing iron concentration (Matsubara et al. 1990; Ohtani et al.

1991). Our data show a similar trend, but the Fe^{3+} concentration must also be taken into account. We fit our cell volume data to the linear correlation

$$V = An_{Fe} + B(n_{Fe^{3+}}/n_{Fe}), \quad (1)$$

where n_{Fe} is the number of iron atoms per three oxygen anions and $n_{Fe^{3+}}/n_{Fe}$ is the relative number of Fe^{3+} atoms ($Fe^{3+}/\sum Fe$). The highest correlation coefficient was found when data from the nine runs in the second series were used ($r^2 = 0.93$), while the correlation coefficient decreased dramatically when the data from the first series of runs were added ($r^2 = 0.63$). The data are plotted in Fig. 9, where values of A and B determined from the regression of the second series of run data [$A = 31(4)$ Å^3 and $B = 1516(1)$ Å^3] were used to generate lines of constant $Fe^{3+}/\sum Fe$. The comparison of literature datasets with the present data shows that while there is a general trend that cell volumes increase with both total iron and relative Fe^{3+} concentration, the variation is obscured by additional factors similar to the case of the c/a ratios, perhaps relating to differences in Mg/Si ordering. It is clear, therefore, that cell volumes should not generally be used to determine either Fe content or relative Fe^{3+} concentration in $(Mg,Fe)SiO_3$ majorite.

The cell volume of $(Mg,Fe)(Si,Al)O_3$ majorite is smaller than the corresponding composition of $(Mg,Fe)SiO_3$ majorite with the same total iron and Fe^{3+} concentration (Fig. 9). This most likely reflects the competition of two different effects: the substitution of Al (0.535 Å) for Si (0.400 Å) on the octahedral site to increase the volume, and the substitution of Al for Fe^{2+} (0.78 Å) and Mg^{2+} (0.72 Å) on the octahedral site to decrease the volume, where ionic radii from Shannon (1976) are given in parentheses.

Charge balance in $(Mg,Fe)(Si,Al)O_3$ majorite most likely occurs through the removal of Si on the octahedral site to accommodate the additional positive charge, as seen by a decrease in Si occupancy with increasing Fe^{3+} concentration (Table 4). The excess Si would then be incorporated into a coexisting phase, for example stishovite. Such a substitution requires no cation or anion vacancies, and is consistent with the electron microprobe data combined with the Mössbauer results, which show the crystals to be stoichiometric within experimental error (Table 4).

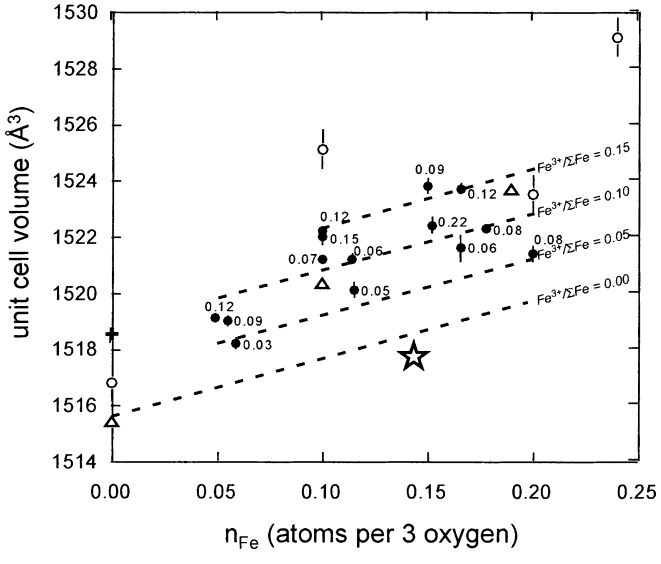

Fig. 9 Variation of unit-cell volume with total iron concentration in $(Mg,Fe)(Si,Al)O_3$ majorite. *Solid circles* indicate the present dataset for $(Mg,Fe)SiO_3$ majorite, where $Fe^{3+}/\sum Fe$ values are indicated next to each data point. Literature data are indicated by *open circles* (Ohtani et al. 1991); *open triangles* (Matsubara et al. 1990); and the *open cross* (Angel et al. 1989). The value from Kato and Kumazawa (1985) of 1506 Å^3 is off scale. *Dotted lines* indicate trends for constant $Fe^{3+}/\sum Fe$, where slopes and intercepts were calculated from multiple regression of Eq. (1) to the second series of runs dataset (U1127–U1220). The *star* indicates the datum for $(Mg,Fe)(Si,Al)O_3$ majorite, which has an $Fe^{3+}/\sum Fe$ value of 0.14

Fe^{2+}–Fe^{3+} electron transfer

The most notable feature of the optical absorption spectra of $(Mg,Fe)SiO_3$ majorite is the presence of Fe^{2+}–Fe^{3+} charge transfer bands (Fig. 6). The integrated intensity, which reflects the number of cation pairs participating in electron transfer, increases with increasing Fe^{3+} concentration (Fig. 10). Extrapolation of the linear relation passes through the origin, suggesting that the proportion of Fe^{3+} atoms participating in electron transfer out of the total number of Fe^{3+} atoms remains constant.

Fe^{2+}–Fe^{3+} electron transfer most likely takes place over the shared edge between dodecahedral sites (occupied by Fe^{2+}) and octahedral sites (occupied by

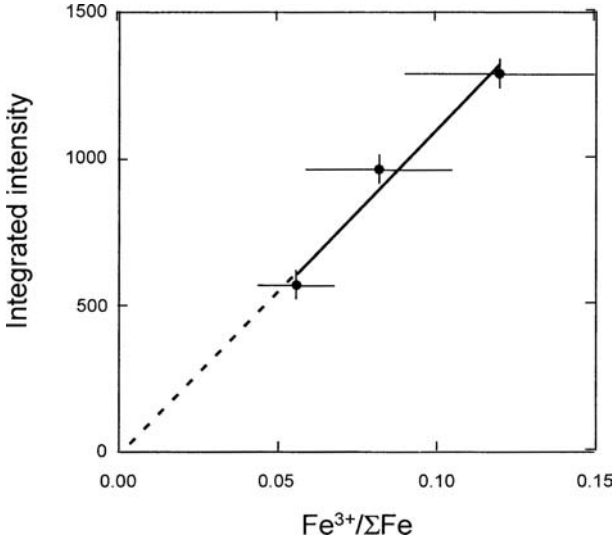

Fig. 10 Variation of integrated intensity of Fe^{2+}–Fe^{3+} charge transfer bands with relative Fe^{3+} concentration from optical absorption spectra of $Mg_{0.85}Fe_{0.15}SiO_3$ majorite. The *solid line* represents a linear regression of the data, where the extrapolated line (*dotted*) passes very close to the origin

Fe^{3+}). The shortest Fe^{2+}–Fe^{3+} distance in $Mg_{0.85}Fe_{0.15}SiO_3$ majorite between D1 and Oc1 is 3.07 Å, while the minimum distance between D1 and Oc2 is 3.30 Å, as calculated from the cell parameters. Both interatomic distances are within the range observed for Fe^{2+}–Fe^{3+} electron transfer, although 3.30 Å is at the upper end (Burns 1993). Keppler and McCammon (1996) suggested that the large linewidth of the Fe^{2+}–Fe^{3+} electron transfer band might indicate that Fe^{3+} substitutes on both octahedral sites, and that electron transfer takes place over both D1–Oc1 and D1–Oc2 shared edges. The large linewidths of the Fe^{3+} doublets in the Mössbauer data from the present work support this suggestion. Although no optical absorption data were collected for (Mg,Fe)(Si,Al)O_3 majorite, it is likely that electron transfer between Fe^{2+} and Fe^{3+} also takes place, since site distribution of Fe^{2+} and Fe^{3+} is similar to that for (Mg,Fe)SiO_3 majorite.

Centre shifts derived from the Mössbauer data indicate that Fe^{2+} and Fe^{3+} occur as discrete oxidation states, i.e., that there is no evidence for iron atoms with intermediate valence. This indicates either that electron transfer between Fe^{2+} and Fe^{3+} involves a negligible number of Fe^{2+}–Fe^{3+} pairs, or that it occurs faster than the mean lifetime of the ^{57}Fe excited state ($\sim 10^{-7}$ s). The latter is more likely, based on comparison with other mixed valence minerals (Burns 1993; Amthauer and Rossman 1984).

Implications for the transition zone

Results from the present work have shown that the relative Fe^{3+} concentration in (Mg,Fe)SiO_3 majorite increases with increasing oxygen fugacity, and that the presence of Al does not increase Fe^{3+} concentration as in the perovskite structure, but may even decrease it slightly. Current studies suggest that the oxygen fugacity in the bulk transition zone is relatively low, based on arguments of reduced volume of ferric iron in garnet (Wood et al. 1990) and the ability of all transition zone phases to accommodate ferric iron (O'Neill et al. 1993a). The results of this work, therefore, would imply a relatively low concentration of Fe^{3+} in (Mg,Fe)(Si,Al)O_3 majorite, which, combined with studies that show similar concentrations of Fe^{3+} in wadsleyite and ringwoodite (O'Neill et al. 1993a), would indicate that the bulk Fe^{3+} concentration in the transition zone is small. Since the value of $Fe^{3+}/\sum Fe$ determined for the upper mantle is also low (2.3%: O'Neill et al. 1993b), an isochemical bulk upper mantle and transition zone with respect to iron oxidation state would be consistent with the present results.

There is a significant increase in the concentration of Fe^{3+} below the transition zone–lower mantle boundary. Even in the absence of Al, (Mg,Fe)SiO_3 perovskite contains approximately twice the concentration of Fe^{3+} than (Mg,Fe)SiO_3 majorite under comparable conditions (McCammon 1998; Lauterbach et al. 2000). When (Mg,Fe)(Si,Al)O_3 majorite transforms to (Mg,Fe)(Si,Al)O_3 perovskite, thereby increasing the Al concentration in the perovskite phase (e.g., Wood 2000), $Fe^{3+}/\sum Fe$ is predicted to reach approximately 50%, based on a pyrolite bulk composition (Lauterbach et al. 2000). This high concentration of Fe^{3+} is independent of oxygen fugacity, and has been observed even for samples synthesized in equilibrium with metallic Fe.

The increase in Fe^{3+} concentration within the lower mantle can occur without a discontinuity in oxygen fugacity between the transition zone and lower mantle. If the lower mantle were also relatively reduced, oxidation of Fe^{2+} to Fe^{3+} could occur through disproportionation ($Fe^{2+} \rightarrow Fe^{3+} + Fe^0$), as observed in experiments (e.g., Lauterbach et al. 2000) or through interaction with volatiles. Another possibility is through subducted material, where oxygen fugacity may be higher (e.g., Wood et al. 1990). Based on the results of the present study, majorite within an oxidized subducted slab would incorporate more Fe^{3+} than the surrounding bulk mantle, and provide a mechanism for the transport of oxygen into the deep mantle.

Acknowledgements This project arose out of preliminary work by Hugh O'Neill, David Rubie, Dante Canil, Charles Geiger, Charles Ross II and Friedrich Seifert on the crystal structure and Mössbauer spectra of (Mg,Fe)SiO_3 majorite. The manuscript was improved significantly by the comments of two anonymous reviewers. NLR acknowledges support of NERC grant GR3/11764. Most of the high-pressure experiments were performed by NLR at the Bayerisches Geoinstitut under the EU TMR – Large Scale Facilities programme (Contract no. ERBFMGECT980111 to D.C. Rubie).

References

Akaogi M, Akimoto S (1977) Pyroxene–garnet solid-solution equilibria in the systems $Mg_4Si_4O_{12}$–$Mg_3Al_2Si_3O_{12}$ and $Fe_4Si_4O_{12}$–$Fe_3Al_2Si_3O_{12}$ at high pressures and temperatures. Phys Earth Planet Int 15: 90–106

Amthauer G, Rossman GR (1984) Mixed valence of iron in minerals with cation clusters. Phys Chem Miner 11: 37–51

Amthauer G, Annersten H, Hafner SS (1976) The Mössbauer spectrum of ^{57}Fe in silicate garnets. Z Kristologe 143: 14–55

Angel RJ, Finger LW, Hazen RM, Kanzaki M, Weidner DJ, Liebermann RC, Veblen DR (1989) Structure and twinning of single-crystal $MgSiO_3$ garnet synthesized at 17 GPa and 1800 °C. Am Mineral 74: 509–512

Angel RJ, McCammon CA, Woodland AB (1998) Structure, ordering and cation interactions in Ca-free $P2_1/c$ clinopyroxenes. Phys Chem Miner 25: 249–258

Burns RG (1993) Mineralogical applications of crystal-field theory, 2nd ed. Cambridge University Press, Cambridge, UK

De Grave E, Van Alboom A (1991) Evaluation of ferrous and ferric Mössbauer fractions. Phys Chem Miner 18: 337–342

Geiger CA, Armbruster T, Lager GA, Jiang GA, Lottermoser W, Amthauer G (1992) A combined temperature-dependent ^{57}Fe Mössbauer and single-crystal X-ray diffraction study of synthetic almandine: evidence for the Gol'danskii-Karagin effect. Phys Chem Miner 19: 121–126

Hatch DM, Ghose S (1989) Symmetry analysis of the phase transition and twinning in $MgSiO_3$ garnet: implications to mantle mineralogy. Am Mineral 74: 1221–1224

Irifune T, Ringwood AE (1987) Phase transformations in primitive MORB and pyrolite compositions to 25 GPa and some geophysical implications. In: Manghnani MH, Syono Y (eds)

High-pressure research in mineral physics. Terra Scientific, Tokyo, pp 231–242
Ito E, Takahashi E (1987) Ultrahigh-pressure phase transformations and the constitution of the deep mantle. In: Manghnani MH, Syono Y (eds) High-pressure research in mineral physics. Terra Scientific, Tokyo, pp 221–229
Kato T (1986) Stability relation of $(Mg,Fe)SiO_3$ garnets, major constituents in the Earth's interior. Earth Planet Sci Lett 77: 399–408
Kato T, Kumazawa M (1985) Garnet phase of $MgSiO_3$ filling the pyroxene–ilmenite gap at very high temperature. Nature 316: 803–805
Keppler H, McCammon CA (1996) Optical absorption spectra of $(Mg,Fe)SiO_3$ majorite. Phys Chem Minerals 23: 94–98
Lauterbach S, McCammon CA, van Aken P, Langenhorst F, Seifert F (2000) Mössbauer and ELNES spectroscopy of $(Mg,Fe)(Si,Al)O_3$ perovskite: a highly oxidised component of the lower mantle. Contrib Mineral Petrol 138: 17–26
Matsubara R, Toraya H, Tanaka S, Sawamoto H (1990) Precision lattice-parameter determination of $(Mg,Fe)SiO_3$ tetragonal garnets. Science 247: 697–699
Mattson SM, Rossman GR (1987) Identifying characteristics of charge transfer transitions in minerals. Phys Chem Miner 14:94–99
McCammon CA (1996) Crystal chemistry of iron-containing perovskites. Phase Transitions 58: 1–26
McCammon CA (1997) Perovskite as a possible sink for ferric iron in the lower mantle. Nature 387: 694–696
McCammon CA (1998) The crystal chemistry of ferric iron in $Mg_{0.95}Fe_{0.05}SiO_3$ perovskite as determined by Mössbauer spectroscopy in the temperature range 80–293 K. Phys Chem Miner 25: 292–300
Ohtani E, Kagawa N, Fujino K (1991) Stability of majorite $(Mg,Fe)SiO_3$ at high pressures and 1800 °C. Earth Planet Sci Lett 102: 158–166
O'Neill HSC, McCammon CA, Canil DC, Rubie DC, Ross II CR, Seifert F (1993a) Mössbauer spectroscopy of transition zone phases and determination of minimum Fe^{3+} content. Am Mineral 78: 456–460
O'Neill HSC, Rubie DC, Canil D, Geiger CA, Ross II CR, Seifert F, Woodland AB (1993b) Ferric iron in the upper mantle and in transition zone assemblages: implications for relative oxygen fugacities in the mantle. In: Takahashi T, Jeanloz R, Rubie DC (eds) Evolution of the earth and planets. American Geophysical Union, Washington DC, pp 73–88
Richmond NC, Brodholt JP (1998) Calculated role of aluminum in the incorporation of ferric iron into magnesium silicate perovskite. Am Mineral 83(9–10): 947–951
Rubie DC (1999) Characterising the sample environment in multianvil high-pressure experiments. Phase Transitions 68: 431–451
Shannon RD (1976) Revised effective ionic radii and systematic studies of interatomic distances in halides and chalcogenides. Acta Crystallogr: (A)32: 751–767
Smith J, Mason B (1970) Pyroxene–garnet transformations in Coorara meteorite. Science 168: 832–833
Speidel DH (1967) Phase equilibria in the system MgO–FeO–Fe_2O_3: the 1300 °C isothermal section and extrapolations to other temperatures. J Am Ceram Soc 50: 243–248
Tomioka N, Fujino K, Ito E, Katsura T, Sharp T, Kato T (2002) Microstructures and structural phase transition in $(Mg,Fe)SiO_3$ majorite. Eur J Mineral 14: 7–14
White WB, Moore RK (1972) Interpretation of the spin-allowed bands of Fe^{2+} in silicate garnets. Am Mineral 57: 1692–1710
Wood BJ (2000) Phase transformations and partitioning relations in peridotite under lower mantle conditions. Earth Planet Sci Lett 174: 341–354
Wood BJ, Bryndzia LT, Johnson KE (1990) Mantle oxidation state and its relationship to tectonic environment and fluid speciation. Science 248: 337–345